Journal of Power Sources 195 (2010) 5081–5088

Contents lists available at ScienceDirect

Journal of Power Sources

journal homepage: www.elsevier.com/locate/jpowsour

Modeling diffusion-induced stress in nanowire electrode structures

Rutooj Deshpande [a,*], Yang-Tse Cheng [a], Mark W. Verbrugge [b]

[a] Chemical and Materials Engineering, University of Kentucky, 177 F Paul Anderson Tower, Lexington, KY 40506, United States
[b] Chemical Sciences and Materials Systems Laboratory, General Motors Global R&D Center, Warren, MI 48090, United States

ARTICLE INFO

Article history:
Received 22 December 2009
Received in revised form 9 February 2010
Accepted 10 February 2010
Available online 18 February 2010

Keywords:
Nanowire electrode
Diffusion-induced stresses
Surface stresses
Surface energy
Strain energy
Durable lithium ion battery electrode

ABSTRACT

There is an intense, worldwide effort to develop durable lithium ion batteries with high energy and power densities for a wide range of applications, including electric and hybrid electric vehicles. One of the critical challenges in advancing lithium ion battery technologies is fracture and decrepitation of the electrodes as a result of lithium diffusion during charging and discharging operations. When lithium is inserted in either the positive or negative electrode, a large volume change on the order of a few to several hundred percent, can occur. Diffusion-induced stresses (DISs) can therefore cause the nucleation and growth of cracks, leading to mechanical degradation of the active electrode materials. Our work is aimed at developing a mathematical model relating surface energy with diffusion-induced stresses in nanowire electrodes. With decreasing size of the electrode, the ratio of surface area to volume increases. Thus, surface energy and surface stress can play an important role in mitigating DISs in nanostructured electrodes. In this work, we establish relationships between the surface energy, surface stress, and the magnitude of DISs in nanowires. We find that DISs, especially the tensile stresses, can decrease significantly due to the surface effects. Our model also establishes a relationship between stress and the nanowire radius. We show that, with decreasing size, the electrode material will be less prone to mechanical degradation, leading to an increase in the life of lithium ion batteries, provided other phenomena are unaffected by increased surface area (e.g., chemical degradation reactions). Also we show that, in the case of nanostructures, surface strain energy is significant in magnitude comparing with bulk strain energy. A mathematical tool to calculate total strain energy is developed that can be used to compare strain energy with the fracture energy of that material in electrode system.

1. Introduction

Lithium diffusion within host electrodes of lithium ion batteries leads to 'Diffusion-Induced Stresses' (DISs), which stimulate mechanical degradation of the electrodes, i.e., pulverization, capacity fading, and decrease in battery performance. Recently, Chan et al. [1], showed that silicon nanowires can accommodate large strain without pulverization. Due to low discharge potential (relative to a lithium reference) and identified high theoretical charge capacity (4200 mAh g^{-1}) [2], silicon nanowires are of interest for lithium ion battery applications. Several research groups have reported on the use of nanotubes and nanowires of different materials as electrodes in lithium ion batteries. Chen et al. [3] have recently shown that CuO nanowires have high reversible capacity. Earlier, Chan and co-workers [4] proposed that Ge nanowires can be used to construct a high capacity Li ion battery. With decreasing size of the active electrode element the surface area to volume ratio increases; as has been recognized in many publications. When the characteristics dimension of a particle falls below tens of nanometers, the number of atoms on the surface of the particle exceeds those of the bulk [5], and unusual particle properties often result relative to the bulk material, which has given rise to the term nanotechnology in more recent times. Cuenot et al. [6] have clarified the influence of nanowire radius on mechanical properties including the apparent stiffness and tensile modulus. Hence, for nanoscale electrode structures, surface energies, and surface stresses can be expected to have a significant impact on the mechanical properties of electrode materials.

A substantial body of literature is devoted to the modeling of lithium ion batteries using volume-averaged (macro-homogeneous) methods to characterize simultaneously the liquid and solid phase phenomena [7–14]. Prussin [15] made an analogy between thermal stress and DIS and analyzed the transverse stresses developed in a thin plate during mass transfer. Lee and co-workers [16–18] also studied DIS in various systems including thin plates, hollow cylinders, and composites. Garcia et al. [19] developed a numerical framework which describes the spatial distribution of electrochemical fields and stress distribution in porous-electrode microstructures. Christensen and Newman

* Corresponding author. Tel.: +1 859 457 1311; fax: +1 859 323 1929.
E-mail addresses: rutooj.deshpande@uky.edu (R. Deshpande), ycheng@engr.uky.edu (Y.-T. Cheng), mark.w.verbrugge@gm.com (M.W. Verbrugge).

0378-7753/$ – see front matter © 2010 Elsevier B.V. All rights reserved.
doi:10.1016/j.jpowsour.2010.02.021

Nomenclature

List of symbols

r, θ, z	cylindrical coordinates
γ	surface energy per unit area ($J\,m^{-2}$)
$\delta_{\alpha\beta}$	Kroneker delta function
$\sigma^{surf}_{\alpha\beta}$	surface stress ($N\,m^{-1}$)
λ and μ	Lamé constants for isotropic bulk material ($N\,m^{-2}$)
λ^s and μ^s	surface Lamé constants($N\,m^{-1}$)
$\kappa_{\alpha\beta}$	curvature tensor of the surface (m^{-1})
τ^0	residual surface tension under unrestrained conditions (N m)
n_α	normal vector
ε_{ij}	infinitesimal strain tensor
Ω	partial molar volume of the solute ($mol\,m^{-3}$)
R	radius of the cylindrical electrode (m)
ν	Poisson's ratio
E	Young's modulus ($N\,m^{-2}$)
u	radial displacement (m)
σ_r	radial stress ($N\,m^{-2}$)
σ_θ	tangential stress ($N\,m^{-2}$)
σ_z	axial stress ($N\,m^{-2}$)
ε_{rr}	radial strain
$\varepsilon_{\theta\theta}$	tangential strain
ε_{zz}	axial strain
$C(r,t)$	solute concentration at radius r at time t ($mol\,m^{-3}$)
$C_{avg}(r)$	average concentration in the area of radius r ($mol\,m^{-3}$)
$C_{avg}(R)$	average concentration in the area of radius R ($mol\,m^{-3}$)
D	diffusion coefficient of the solute ($m^2\,s^{-1}$)
t	time (s)
x	dimensionless radius
T	dimensionless time
y	dimensionless concentration
J_0 and J_1	Bessel's function of first kind of order 0 and 1 respectively
ξ_r	dimensionless radial stress
ξ_θ	dimensionless tangential stress
ξ_z	dimensionless axial stress
E_{Total}	total elastic energy per unit length stored in the cylinder of radius R and height h ($J\,m^{-1}$)
E_{bulk}	strain energy per unit length stored due to bulk deformation ($J\,m^{-1}$)
$E_{surface}$	strain energy per unit length stored due to surface deformation ($J\,m^{-1}$)
e(r)	strain energy density ($J\,m^{-3}$)
$\prod_{bulk}$	dimensionless bulk strain energy
$\prod_{surface}$	dimensionless surface strain energy

[20,21] and Zhang et al. [22,23] simulated intercalation induced stresses within single particles to capture salient features of the governing electrochemistry and solid mechanics taking place in lithium ion batteries. At the nanoscale, surface effects mentioned above are prominent, which has prompted the inclusion of surface mechanics in within the analysis of DIS of spherical electrode particles [24].

In this paper, we couple DISs and surface stresses so as to elucidate their combined effects on the mechanical behavior of nanowire electrodes; our approach is similar to that employed for spherical particles [24]. This paper provides a mathematical framework for the investigation of nanowire electrodes. In addition to stress effects surface strain energy also becomes significant relative to that of the bulk at the nanoscale. Strain energy is an important criterion that can be used to determine the mechanical stability of an electrode material. Cheng and Verbrugge [25] analyzed strain energy for spherical particles without considering the effects of surface energy. In this work, we perform a complete strain energy analysis showing that surface strain energy provides a significant contribution in total strain energy for nanowires. Furthermore, the total strain energy can be compared with the fracture energy to derive a condition for crack propagation in electrode materials; the ensuing analysis and approach is new to modeling DIS of nanoscale systems and provides a general framework for the investigation of other nanoscale geometries. The specific results of this analysis should prove helpful in guiding the selection of materials for nanowire electrodes.

2. Stress modeling

The surface stress of a material is related to the surface energy and the strain tensor of a particular geometry of the material. This can be expressed with Gibb's equation [26]:

$$\sigma^{surf}_{\alpha\beta} = \gamma\delta_{\alpha\beta} + \frac{\partial\gamma}{\partial\varepsilon_{\alpha\beta}} \tag{1}$$

where γ is surface energy per unit area, $\varepsilon_{\alpha\beta}$ (1) is a 2×2 surface strain tensor, and $\delta_{\alpha\beta}$ is the Kronecker delta function. For liquids, surface stress and γ have the same value because of the high mobility of atoms in fluids. For solids, surface stress and surface energy are not the same because of the finite elasticity of solid surfaces. Under the assumption that the surface adheres to the bulk without slipping, and in the absence of body forces, the equilibrium and constitutive equations for isotropic case can be summarized as follows [26]. In the bulk:

$$\begin{aligned} &\sigma^{bulk}_{ij,j} = 0 \\ &\sigma^{bulk}_{ij} = C_{ijkl}\varepsilon_{kl} = [\lambda\delta_{ij}\delta_{kl} + \mu(\delta_{ik}\delta_{jl} + \delta_{il}\delta_{jk})]\varepsilon_{kl} \end{aligned} \tag{2a}$$

On the surface (or interface):

$$\begin{aligned} &\sigma^{bulk}_{\beta\alpha}n_\beta + \sigma^{surface}_{\beta\alpha,\beta} = 0 \qquad \sigma^{bulk}_{ij}n_jn_i = \sigma^{surface}_{\alpha\beta}\kappa_{\alpha\beta} \\ &\sigma^{surface}_{\alpha\beta} = \tau^0\delta_{\beta\alpha} + 2(\mu^s - \tau^0)\delta_{\beta\gamma}\varepsilon_{\gamma\alpha} \\ &\qquad\qquad +(\lambda^s + \tau^0)\varepsilon_{\gamma\gamma}\delta_{\beta\alpha} \end{aligned} \tag{2b}$$

where λ and μ are the Lamé constants for the isotropic bulk material. The surface/interface can be characterized by surface Lamé constants λ^s and μ^s, which give deformation dependent surface energy. Other symbols denote the following [26]; $\kappa_{\alpha\beta}$ is the curvature tensor of the surface/interface, τ^0 is residual surface tension under unrestrained conditions, n_α is normal vector to surface/interface, and ε_{ij} is infinitesimal strain tensor. It is noted that only certain strain components appear within the constitutive law for surfaces due to the 2×2 nature of the surface stress tensor (i.e., strains normal to the surface are excluded). The Greek indices take on values 1 and 2 while Latin subscripts adopt values 1 through 3. Conventional summation rules apply unless otherwise noted.

For cylindrical structure, i.e., nanowires, we can rewrite this equation as follows:

$$\sigma_\theta = \sigma_{\theta\theta} = \tau^0 + (2\mu^s + \lambda^s - \tau^0)\varepsilon_{\theta\theta} = \tau^0 + K^s\varepsilon_{\theta\theta} \tag{3}$$

The bulk of the nanowire will be assumed to be an isotropic, linearly elastic solid. Using the analogy between thermal stresses [27,28] and DISs, we can write,

$$\varepsilon_{rr} - \frac{\Omega}{3}C = \frac{1}{E}(\sigma_r - \nu(\sigma_\theta + \sigma_z)) \tag{4}$$

Similarly,

$$\varepsilon_{\theta\theta} - \frac{\Omega}{3}C = \frac{1}{E}(\sigma_\theta - \nu(\sigma_r + \sigma_z)) \tag{5}$$

where E is the Young's modulus, C is the molar concentration, and Ω is the partial molar volume of the solute. Depending upon the axial stress conditions, the axial strain can have three possibilities.

i. If the electrode is a long wire, the strain in the z-direction may be negligible. This is the plane strain condition, i.e., $\varepsilon_{zz} = 0$.
ii. If nanowires are free at the ends, $F_z = \int_0^R 2\pi r\sigma_z dr = 0$. This is the generalized plane strain condition.
iii. If there is no axial stress present, $\sigma_z = 0$. This is the plane stress condition.

We further assume that the physicochemical properties associated with the linear elastic solid are independent of concentration.

In practice, nanowires electrodes are long wires grown on a substrate and thus one of the ends of the wire is always attached to the substrate. The other end is free to expand. Changes in stress condition at the fixed end have effect on the stress distribution near that end. But according to Saint-Venant's principle [28], the effects on stress due by the fixed end are expected to diminish with distance from the fixed end. Since the other end is free to expand, we can assume that long nanowires with a fixed end are under the generalized plane strain condition (i.e., condition ii).

Since atomic diffusion in solids is a much slower process than elastic deformation, mechanical equilibrium is established much faster than that of diffusion. Mechanical equilibrium is, therefore, treated as a static equilibrium problem [24]. In the absence of any body force, the equation for static mechanical equilibrium in the bulk of a cylinder is

$$\frac{d\sigma_r}{dr} + \frac{\sigma_r - \sigma_\theta}{r} = 0 \tag{6}$$

For infinitesimally small deformation, the radial and tangential strain of cylindrical particle can be related to radial displacement u, by the relation:

$$\varepsilon_{rr} = \frac{du}{dr}, \quad \varepsilon_{\theta\theta} = \frac{u}{r} \tag{7}$$

There is no displacement at the center, and $u(0) = 0$. Furthermore, the radial stress σ_r must satisfy mechanical equilibrium at the surface $r = R$ (where, R is the radius of the cylinder) [26]:

$$\sigma_r|_{r=R} = -\frac{\sigma_\theta^{\text{surface}}}{R} \tag{8}$$

Using these conditions, Eqs. (3)–(8), and no further assumptions, we can express the stress components as follows:

$$\sigma_r = \frac{\Omega}{3}E^*\left[\frac{1}{2}\left\{\frac{1-((2\mu^s+\lambda^s-\tau^0)/ER)(1+\nu)}{1+((2\mu^s+\lambda^s-\tau^0)/ER)\,\nu^*}\right\}C_{avg}(R) - \frac{1}{2}C_{avg}(r)\right] - \left[\frac{\tau^0/R}{1+((2\mu^s+\lambda^s-\tau^0)/ER)\,\nu^*}\right] \tag{9}$$

$$\sigma_\theta = \frac{\Omega}{3}E^*\left[\frac{1}{2}\left\{\frac{1-((2\mu^s+\lambda^s-\tau^0)/ER)(1+\nu)}{1+((2\mu^s+\lambda^s-\tau^0)/ER)\,\nu^*}\right\}C_{avg}(R) + \frac{1}{2}C_{avg}(r) - C(r)\right] - \left[\frac{\tau^0/R}{1+((2\mu^s+\lambda^s-\tau^0)/ER)\,\nu^*}\right] \tag{10}$$

$$\sigma_z = j\left[\frac{\Omega}{3}E^*\left[\left\{q^* + \nu\frac{1-((2\mu^s+\lambda^s-\tau^0)/ER)(1+\nu)}{1+((2\mu^s+\lambda^s-\tau^0)/ER)\,\nu^*}\right\}C_{avg}(R) - C(r)\right] - 2\upsilon\left[\frac{\tau^0/R}{1+((2\mu^s+\lambda^s-\tau^0)/ER)\,\nu^*}\right]\right] \tag{11}$$

where $C_{avg}(r) = (2/r^2)\int_0^r C(r')r'dr'$ is the average concentration inside a cylinder of unit length and radius r. Here,

i. For the plane strain condition:

$$E^* = \frac{E}{1-\nu}, \quad \nu^* = (1-2\nu)(1+\nu), \quad q^* = 0, j = 1 \tag{12}$$

ii. For the generalized plane strain condition:

$$E^* = \frac{E}{1-\nu}, \quad \nu^* = (1-2\nu)(1+\nu), \quad q^* = (1-\nu), \quad j = 1 \tag{13}$$

iii. For the plane stress condition:

$$E^* = E, \quad \nu^* = (1-\nu), \quad q^* = (1-\nu), \quad j = 0 \tag{14}$$

The stress components contain surface energy and surface tension terms, and the following definitions are used to streamline notation:

$$S_1 = \left[\frac{1-((2\mu^s+\lambda^s-\tau^0)/ER)(1+\nu)}{1+((2\mu^s+\lambda^s-\tau^0)/ER)\,\nu^*}\right], \quad S_2 = -\left[\frac{\tau^0/R}{1+((2\mu^s+\lambda^s-\tau^0)/ER)\,\nu^*}\right] \tag{15}$$

Note that the quantities μ^s, λ^s and τ^0 multiply onto $C_{avg}(R)$, which is a time-dependent quantity. The term S_2 has dimensions of stress and the negative sign ensures that it's always compressive relative to the radial, tangential, or axial stress. The radius R in the denominator makes clear that as the size of the electrode particle is reduced, S_2 will have a greater effect on the principal stresses. Thus, in nanoscale structures, surface tension can be expected to play an important role in affecting DISs.

Lithium ions diffuse in or out of the electrode during charging or discharging. For dilute solutes within the cylindrical host material, the solute (lithium ion) concentration is governed by the diffusion equation:

$$\frac{\partial C}{\partial t} = D\left(\frac{\partial^2 C}{\partial r^2} + \frac{1}{r}\frac{\partial C}{\partial r}\right) \tag{16}$$

There are two possible ways of operating a battery:

a. Potentiostatic operation: the electrode is surrounded by a constant lithium ion concentration.
b. Galvanostatic operation: the current, thus the ionic flux at the surface of the electrode, is a constant.

Here, we assume that the electrode surface is surrounded by an invariant lithium ion concentration C_R (reflecting facile electrochemical kinetics and a porous-electrode system dominated by solute-diffusion resistance [24,25]). The case of galvanostatic charging is discussed in details in the 'supplementary information' section. We assume the initial lithium ion concentration inside the electrode is C_0. In addition, the concentration at the center is finite. The initial and boundary conditions are, therefore,

$$C(r, 0) = C_0, \quad \text{for } 0 \le r \le R$$

$$C(R, t) = C_R, \quad \text{for } t \ge 0$$

$$C(0, t) = \text{finite}, \quad \text{for } t \ge 0$$

Eq. (16) can be made dimensionless with the following:

$$x = \frac{r}{R}, \quad T = \frac{Dt}{R^2}, \quad y = \frac{C - C_0}{C_R - C_0} \tag{17}$$

Hence,

$$\frac{\partial y}{\partial T} = \left(\frac{\partial^2 y}{\partial x^2} + \frac{1}{x}\frac{\partial y}{\partial x}\right) \tag{18}$$

The initial and boundary conditions can be rewritten in the dimensionless form as follows:

$$y(x,0) = 0, \quad \text{for } 0 \le x \le 1$$

$$y(1,T) = 1, \quad \text{for } T \ge 0$$

$$y(0,T) = \text{finite}, \quad \text{for } T \ge 0 \tag{19}$$

The analytic solution of this problem is well known and is reproduced here [27,29]:

$$y(x,T) = 1 - 2\sum_{n=1}^{\infty}\left\{\frac{e^{-\lambda_n^2 T} J_0(\lambda_n x)}{\lambda_n J_1(\lambda_n)}\right\} \tag{20}$$

where J_0 and J_1 are the Bessel functions of the first kind of order 0 and 1 respectively, and λ_n are the n solutions of equation $J_0(\lambda_n) = 0$. The average concentrations can be written as follows:

$$y_{avg}(x) = \frac{C_{avg}(r) - C_0}{C_R - C_0} = \left(1 - \frac{4}{x}\sum_{n=1}^{\infty}\left\{\frac{e^{-\lambda_n^2 T} J_1(\lambda_n x)}{\lambda_n^2 J_1(\lambda_n)}\right\}\right) \tag{21}$$

$$y_{avg}(1) = \frac{C_{avg}(R) - C_0}{C_R - C_0} = \left(1 - 4\sum_{n=1}^{\infty}\left\{\frac{e^{-\lambda_n^2 T}}{\lambda_n^2}\right\}\right) \tag{22}$$

We can now recast the stress components in dimensionless form:

$$\begin{aligned}\xi_r &= \frac{\sigma_r}{[(\Omega/3)(E/(1-\nu))(C_R - C_0)]} \\ &= \left[\frac{1}{2}\bar{\nu}\left[(S_1 - 1)\left(\frac{C_0}{C_0 - C_R}\right) + S_1\left(1 - 4\sum_{n=1}^{\infty}\left\{\frac{e^{-\lambda_n^2 T}}{\lambda_n^2}\right\}\right)\right.\right. \\ &\quad \left.\left. - \left(1 - \frac{4}{x}\sum_{n=1}^{\infty}\left\{\frac{e^{-\lambda_n^2 T} J_1(\lambda_n x)}{\lambda_n^2 J_1(\lambda_n)}\right\}\right)\right] \\ &\quad \left. + \frac{S_2}{[(\Omega/3)(E/(1-\nu))(C_R - C_0)]}\right]\end{aligned} \tag{23}$$

$$\begin{aligned}\xi_\theta &= \frac{\sigma_\theta}{[(\Omega/3)(E/(1-\nu))(C_R - C_0)]} \\ &= \left[\frac{1}{2}\bar{\nu}\left[(S_1 - 1)\left(\frac{C_0}{C_0 - C_R}\right) + S_1\left(1 - 4\sum_{n=1}^{\infty}\left\{\frac{e^{-\lambda_n^2 T}}{\lambda_n^2}\right\}\right)\right.\right. \\ &\quad \left.\left. + \left(1 - \frac{4}{x}\sum_{n=1}^{\infty}\left\{\frac{e^{-\lambda_n^2 T} J_1(\lambda_n x)}{\lambda_n^2 J_1(\lambda_n)}\right\}\right)\right] \\ &\quad - \bar{\nu}\left(1 - 2\sum_{n=1}^{\infty}\left\{\frac{e^{-\lambda_n^2 T} J_0(\lambda_n x)}{\lambda_n J_1(\lambda_n)}\right\}\right) \\ &\quad \left. + \frac{S_2}{[(\Omega/3)(E/(1-\nu))(C_R - C_0)]}\right]\end{aligned} \tag{24}$$

$$\begin{aligned}\xi_z &= \frac{\sigma_z}{[(\Omega/3)(E/(1-\nu))(C_R - C_0)]} \\ &= j\left[\left[(q^* + \nu S_1 - 1)\left(\frac{C_0}{C_0 - C_R}\right) + [q^* + \nu S_1]\left(1 - 4\sum_{n=1}^{\infty}\left\{\frac{e^{-\lambda_n^2 T}}{\lambda_n^2}\right\}\right)\right.\right. \\ &\quad \left.\left. - \left(1 - 2\sum_{n=1}^{\infty}\left\{\frac{e^{-\lambda_n^2 T} J_0(\lambda_n x)}{\lambda_n J_1(\lambda_n)}\right\}\right)\right] \\ &\quad \left. + 2\upsilon\frac{S_2}{[(\Omega/3)(E/(1-\nu))(C_R - C_0)]}\right]\end{aligned} \tag{25}$$

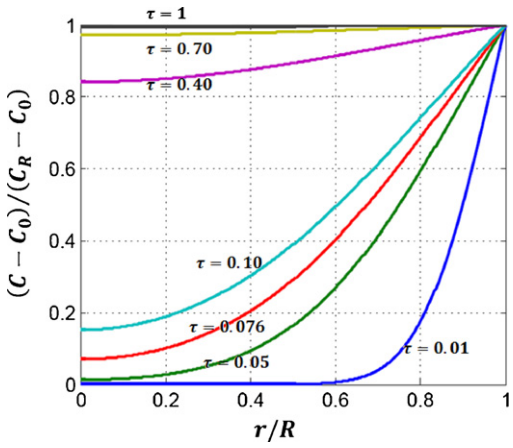

Fig. 1. Lithium ion concentration (Eq. (20)) inside an electrode at different radial locations and times for insertion condition.

For the plane strain condition, $\bar{\nu} = 1$; for the generalized plane strain condition, $\bar{\nu} = 1$; and for the plane stress condition, $\bar{\nu} = (1 - \nu)$. The quantities ξ_r, ξ_z, and ξ_θ represent dimensionless stresses in r, z, and θ-directions, respectively. On charge, lithium ions will be inserted into the negative electrode and extracted from the positive electrode; the opposite hold true for discharge.

We can plot dimensionless concentration at different radial positions and time using Eq. (20) as depicted in Fig. 1. First, we consider a case of an electrode with a large diameter. There will be neither surface tension nor surface energy effects on the stresses. In this case, $S_1 = 1$ and $S_2 = 0$. We plot dimensionless radial and tangential stresses. We find that radial stresses (solid lines, Fig. 2), in both plane strain and generalized plane stress conditions are similar. Similarly, tangential stresses (solid lines, Fig. 3), in these two conditions are identical. We assume that the initial concentration of solute (lithium ion) inside the electrode is $C_0 = 0$. Similarly, we plot radial and tangential stress for plane stress condition for a large diameter electrode. In all the three cases, the radial stress at the center initially increases, reaches a maximum when $T = Dt/R^2 = 0.076$, and then decreases gradually until the electrode reaches saturation concentration. The radial stress is always tensile if there are no surface effects. The tangential stress is tensile at the center and compresssive at the surface. The magnitude of radial and tangential stress are the same at the center. The tangential stress maxima occures at the surface at time zero. At time zero and $r = R$, $C_{avg}(R) = C_{avg}(r) \cong 0$, and $C(r) = C_R$. From Eqs. (10) and (13), for the plane strain and generalized plane strain condition:

$$\frac{\sigma_\theta}{[(\Omega/3)(E/(1-\nu))C_R]}|_{\max} \cong -\bar{\nu} + \frac{S_2}{[(\Omega/3)(E/(1-\nu))C_R]} \tag{26}$$

Here, $\bar{\nu}$ value is same as mentioned in Eq. (25) depending upon axial loading condition. Eq. (26) gives the maximum tangential stress that the electrode material will be subjected to. The maximum tangential stress will vary depending upon value of S_2 and the axial loading condition. It can be used as an important parameter to design an electrode material.

In the absense of surface effects ($S_1 = 1$ and $S_2 = 0$), the equation system is symmetric, and mirror opposite conclusions hold for the case of deinsertion (i.e., replacing tensile stress by compressive stress). This stress distribution is independent of the particle

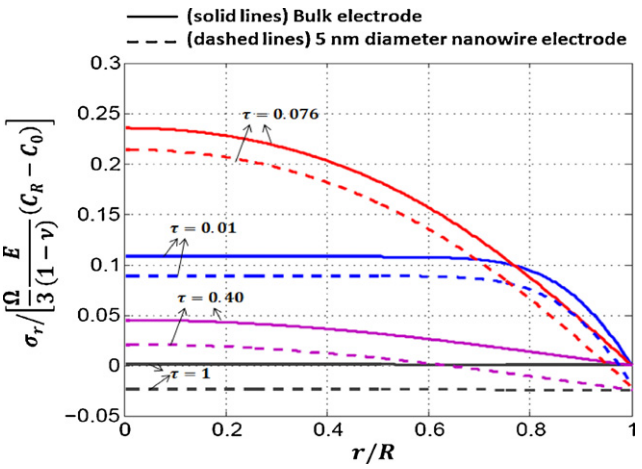

Fig. 2. Radial stress (Eq. (23)) inside an electrode at different radial locations at different time. This is for generalized plane strain condition. Solid lines represents stresses in large electrode i.e., no surface effects are considered ($S_1 = 1$ and $S_2 = 0$). Dashed lines represent stresses in 5 nm diameter nanowire electrodes i.e., surface effect is significant ($S_1 = 0.9855$ and $(S_2/[(\Omega/3)(E/(1-\nu))C_R]) = 0.0174$).

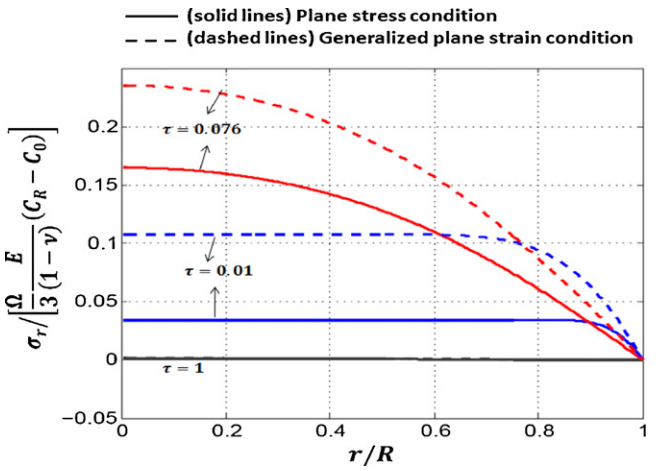

Fig. 4. Radial stress inside an electrode at different radial locations and times. Solid lines represent plane stress condition. Dashed lines represent generalized plane strain condition. No surface effects are considered.

radius; with proper time and radius scaling, the stress distribution is idential for all particle radii.

We see, from Figs. 4–6, that all three stresses are dependant on the axial loading condition of the electrode. Furthermore, the radial and tangential stresses for plane strain and generalized plane strain condition are exactly the same. In contrast, the axial stresses are significantly different in the two cases. The plane stress condition leads to different radial and tangential stresses than plane strain conditions (see Figs. 4 and 5).

We now consider the influence of small electrode diameters and surface effects on stress distribution. For evaluating the surface effects, the parameters values of Ref. [24] are employed directly, making it straightforward to compare spherical and cylindrical electrodes. Specifically, $E = 10$ GPa, $\nu = 0.3$, and $(\Omega/3)C_R = 0.08$. We take surface tension value as $1\,\mathrm{J\,m^{-2}}$ and $(2\,\mu^s + \lambda^s)$ is $5\,\mathrm{N\,m^{-1}}$, which is of same order of magnitude as surface modulus values of Al and Si [28]. With these values, we get $S_1 = 0.9855$ and $(S_2/[(\Omega/3)(E/(1-\nu))C_R]) = 0.0174$. The plots obtained of dimensionless radial and tangential stress vs. radial distance for a 5 nm cylindrical wire are shown in Figs. 2 and 3 (dashed lines). These

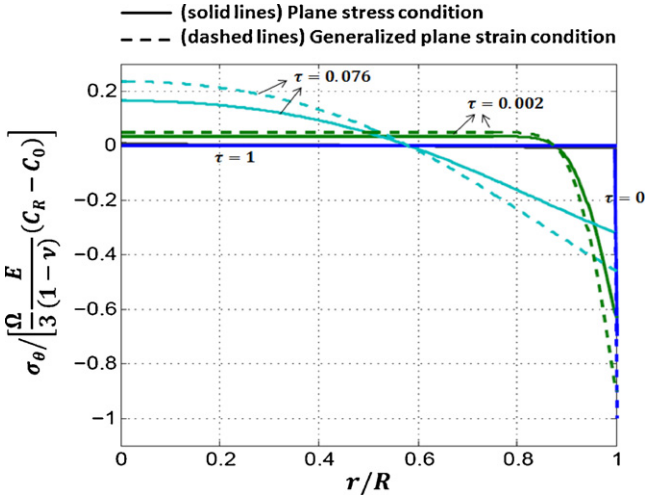

Fig. 5. Tangential stress (Eq. (24)) inside an electrode at different radial locations and times. Solid lines represent plane stress condition. Dashed lines represent generalized plane strain condition. No surface effects are considered.

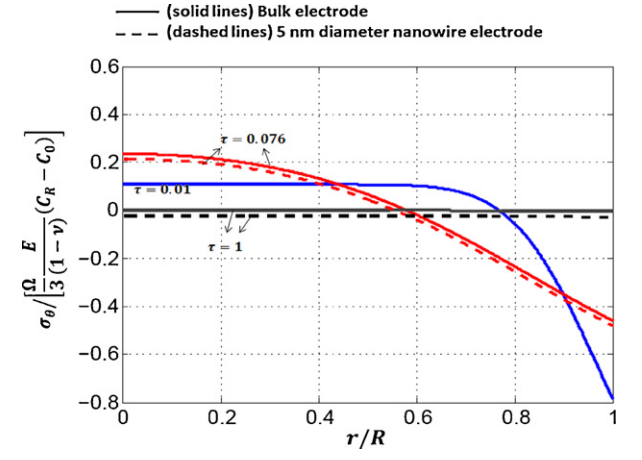

Fig. 3. Tangential stress (Eq. (24)) inside an electrode at radial locations and times. This is for generalized plane strain condition. Solid lines represents stresses in large electrode i.e., no surface effects are considered ($S_1 = 1$ and $S_2 = 0$). Dashed lines represent stresses in 5 nm diameter nanowire electrodes i.e., surface effect is significant ($S_1 = 0.9855$ and $(S_2/[(\Omega/3)(E/(1-\nu))C_R]) = 0.0174$).

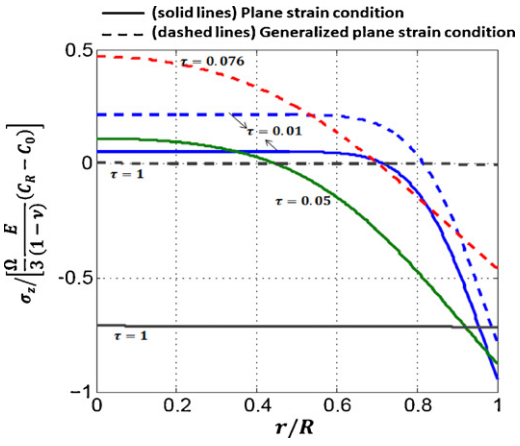

Fig. 6. Axial stress (Eq. (25)) inside an electrode at radial locations and times. Solid lines represent plane strain condition. Dashed lines represent generalized plane strain condition. No surface effects are considered.

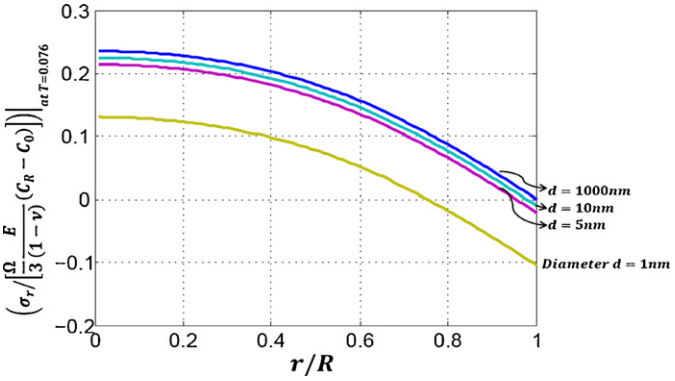

Fig. 7. Radial stress at a dimensionless time $T = 0.076$ for electrodes with different diameters. The results are for plane strain and generalized plane strain conditions.

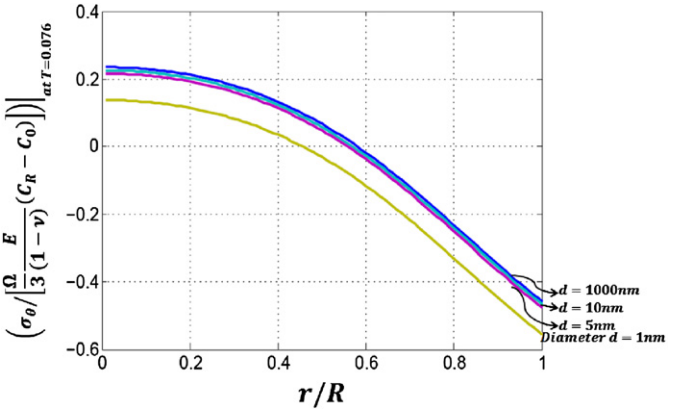

Fig. 8. Tangential stress at dimensionless time $T = 0.076$ for electrodes with different diameters. The results are for plane strain and generalized plane strain conditions.

are for plane strain conditions in axial direction. Similar plots can be obtained for the other two axial boundary conditions. In both the Figs. 2 and 3, by comparing solid lines and dashes lines, it can be observed that at the nanoscale, there is a significant decrease in both radial and tensile stresses.

We plot radial and tangential stress at time $T = 0.076$ for cylindrical electrodes of different diameters in Figs. 7 and 8, respectively. For insertion, the maximum tangential stress is always compressive and its magnitude is increased as the particle radius is decreased. It can be observed that, as radius decreases, the effect of surface tension becomes much more significant. These results make it clear that when the influence of surface tension is incorporated, smaller (nanoscale) wires see a more compressive stress environment, which would decrease the probability of crack formation due to tensile stress.

3. Strain energy

Due to deformation, elastic strain energy is stored in the electrode. This energy is a driving force for crack propagation in the electrode. Ref. [25] overviews a strain energy analysis for spherical particles. For nanoscale particles, the surface strain energy also has a significant contribution to total energy. The total strain energy for the particle can be expressed as follows:

$$E_{\text{total}} = E_{\text{bulk}} + E_{\text{surface}} \tag{27}$$

From the stresses, we can calculate the bulk strain energy per unit volume or bulk strain energy density $e(r)$ accumulated as a result of the elastic deformation for the isotropically deformed cylinder as follows [28]:

$$e(r) = \frac{1}{2E}(\sigma_r^2 + \sigma_\theta^2 + \sigma_z^2) - \frac{\nu}{E}(\sigma_r\sigma_\theta + \sigma_\theta\sigma_z + \sigma_z\sigma_r) \tag{28}$$

The total bulk strain energy can be obtained by integrating the strain energy density over the entire volume. The bulk strain energy per unit length of the wire can be obtained as follows:

$$E_{\text{bulk}} = 2\pi \int_0^R e(r) r dr \tag{29}$$

$$E_{\text{bulk}} = 2\pi \int_0^R \left[\tfrac{1}{2E}(\sigma_r^2 + \sigma_\theta^2 + \sigma_z^2) - \tfrac{\nu}{E}(\sigma_r\sigma_\theta + \sigma_\theta\sigma_z + \sigma_z\sigma_r)\right] r dr$$

In dimensionless form:

$$\Pi_{\text{bulk}} = \frac{E_{\text{bulk}}}{\pi R^2 E((\Omega/3)(C_R - C_0)/(1-\nu))^2} = \int_0^1 [(\xi_r^2 + \xi_\theta^2 + \xi_z^2) - 2\nu(\xi_r\xi_\theta + \xi_\theta\xi_z + \xi_z\xi_r)] x dx \tag{30}$$

Along with bulk strain energy, surface strain energy is also stored in the electrode. To derive an expression for surface strain energy density, we consider a cylinder of original diameter R that is stretched to a new radius $R + \Delta R$ (cf. Fig. 9). The surface stress has two parts (see Eq. (3)). The contribution to the total surface energy as a result of the increase in radius can be expressed as follows:

$$2\pi h(R + \Delta R)\tau^0 - 2\pi hR\tau^0 = 2\pi h\Delta R\tau^0 = 2\pi hR\frac{\Delta R}{R}\tau^0 = 2\pi hR\varepsilon_\theta\tau^0 \tag{31}$$

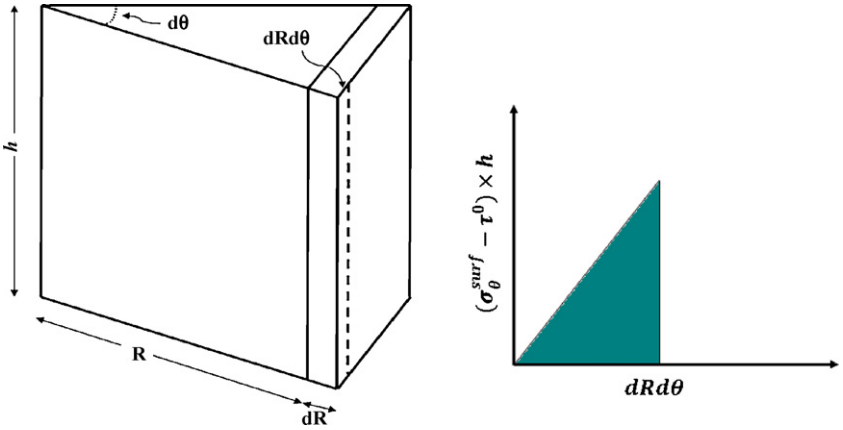

Fig. 9. A schematic illustration of contributions to strain energy.

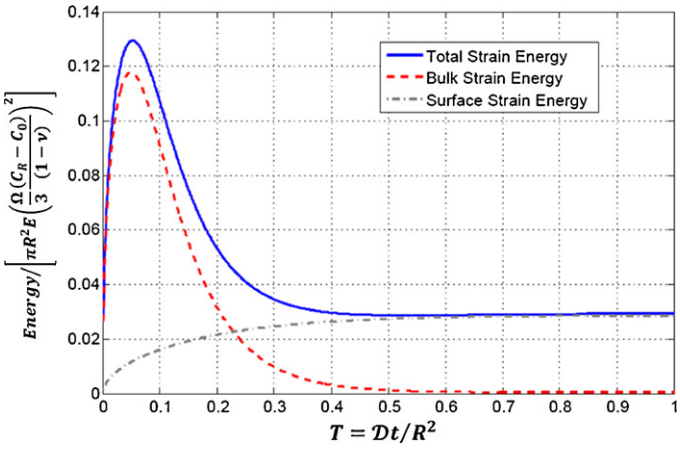

Fig. 10. Bulk strain energy, surface strain energy, total strain energy with time for a 5-nm electrode subject to the generalized plane strain condition.

The contribution of the surface tension τ^0 to the surface strain energy density is, therefore,

$$\frac{2\pi h(R+\Delta R)\tau^0 - 2\pi Rh\tau^0}{2\pi Rh} = \frac{2\pi h\Delta R\tau^0}{2\pi Rh} = \varepsilon_\theta \tau^0 \tag{32}$$

We now consider the contribution of $K^s\varepsilon_\theta$ to the surface-strain energy density. With the assistance of Fig. 9, we note that a force balance yields:

$$(\sigma^{\text{surface}} - \tau^0)h = K^s\varepsilon_\theta h \tag{33}$$

The work is the shaded area in Fig. 9 and is given by

$$\frac{1}{2}(\sigma^{\text{surface}} - \tau^0)hdRd\theta = \frac{1}{2}K^s\varepsilon_\theta hdRd\theta \tag{34}$$

The work per unit area is, therefore, given by

$$\frac{1/2(\sigma^{\text{surface}} - \tau^0)hdRd\theta}{hdRd\theta} = \frac{1/2K^s\varepsilon_\theta hdRd\theta}{hdRd\theta} = \frac{1}{2}K^s\varepsilon_\theta \tag{35}$$

Thus total surface strain energy can be written as,

$$\text{Total surface strain energy per unit length} = 2\pi R\left(\tau^0\varepsilon_0 + \frac{1}{2}K^s\varepsilon_\theta^2\right) \tag{36}$$

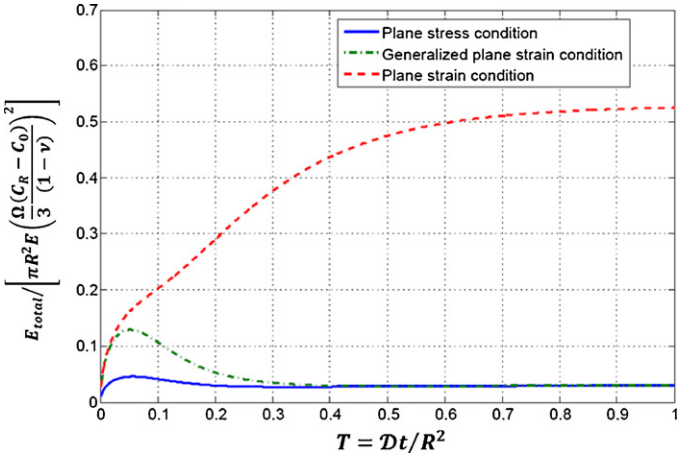

Fig. 11. Total strain energy variation with time for a 5-nm electrode. All the three loading conditions are taken investigated, and it is clear that the total strain energy stored varies with the axial loading condition.

To compare with bulk strain energy, this surface strain energy is normalized with the same quantity:

$$\prod_{\text{surface}} = \frac{2\pi R(\tau^0\varepsilon_0 + (1/2)K^s\varepsilon_\theta^2)}{\pi R^2 E((\Omega/3)(C_R - C_0)/(1-\nu))^2} = \frac{2(\tau^0\varepsilon_0 + (1/2)K^s\varepsilon_\theta^2)}{RE((\Omega/3)((C_R - C_0)/(1-\nu)))^2} \tag{37}$$

Thus total strain energy stored in the electrode due to volumetric expansion is addition of the bulk and surface strain energy. Fig. 10 shows the dimensionless bulk strain energy, surface strain energy, and total strain energy stored in 5 nm cylindrical electrode due to lithium intercalation in generalized plane strain condition. We can see that surface strain energy has a considerable effect on the total strain energy. In addition, it can be inferred that the surface strain energy has a comparable magnitude to the bulk strain energy for the 5 nm electrode in all the three cases. This confirms the fact that for representative parameters values and nanoscale electrode dimensions, the surface effects are considerably strong and can mitigate deleterious efforts of DISs in terms of fracture propagation; hence, from a fracture perspective, nanoscale electrodes can be expected to provide higher cycle life than electrode constructed with large particles. Experiments with nanowire electrodes support this. For example, Chan et al. [1], showed that silicon nanowires can accommodate large strain without pulverization. Nano-wired structured electrodes of different material like Si, Sn, TiO_2 have been experimented. These experiments also confirm better behavior of nanowire electrodes than bulk electrodes [30,4,31–36]. These results also depend upon the surface and material properties of the electrode material [37], and we have not considered potential deleterious chemical reactions that are enhanced by increased electrode surface area, such as solvent reduction on carbon negatives [38]. Using this mathematical model, we can select the best possible material for the electrode, in terms of resistance to crack propagation, by comparing this total energy calculated with the surface energy for cracking. Thus at nanoscale, not only bulk strain energy but surface strain energy should be considered for predicting the initiation and propagation of fracture.

Fig. 11 shows that variation of total strain energy in all the axial loading conditions. The difference in the nature of strain energy profiles in all the three cases is due to the different nature of axial stress. From Fig. 11 we can see that, in case of the plane stress and generalized plane strain condition, strain energy increases initially, reaches a peak value, and then decreases. On the other hand, in case of the plane strain condition, energy increases initially and then a reaches a steady maximum value. The valley seen in the plane strain curve is consistent with the radial and tangential stress maxima. The increase in total energy afterwards is related to the continuous increase in magnitude of axial stress. The electrode subjected to the plane stress condition exhibits less stored strain energy and is thus less prone to cracking as compared to other two cases.

4. Conclusions

1. There can be a significant decrease in the diffusion-induced stress due to surface effects. Furthermore, we find in some cases that the tensile stress is converted to compressive stress, which will inhibit crack formation and in turn reduce mechanical degradation. The results clearly indicate that below a certain wire diameter, the surface effect plays an important role.
2. The importance of the surface strain energy contribution to the total strain energy is established. This leads to a conclusion that for nanostructured materials, the fracture energy should be compared with a total strain energy that includes both bulk and

surface strain energy. Surface strain energy analyses have not been incorporated in previous studies.
3. The importance of the strain or stress boundary conditions along the axial direction of the nanowire electrodes is examined (i.e., plane stress versus plane strain).
4. A mathematical tool is developed for the analysis of stress, strain, and strain energy in cylindrical nanostructured electrodes, which can be employed for materials with known properties. This model can be used to optimize the cylindrical electrode size depending upon the properties to maximize the battery life. It may also be used as a tool for battery life prediction.

Appendix A. Supplementary data

Supplementary data associated with this article can be found, in the online version, at doi:10.1016/j.jpowsour.2010.02.021.

References

[1] C.K. Chan, H. Peng, G. Liu, K. McIlwrath, X.F. Zhang, R.A. Huggins, Y. Cui, Nature Nanotechnology 3 (2008) 31–35.
[2] B.A. Boukamp, G.C. Lesh, R.A. Huggins, Journal of the Electrochemical Society 128 (1981) 725–729.
[3] L.B. Chen, N. Lu, C.M. Xu, H.C. Yu, T.H. Wang, Electrochimica Acta 54 (2009) 4198–4201.
[4] C.K. Chan, X.F. Zhang, Y. Cui, Nano Letters 8 (2007) 307–309.
[5] C. Herring, Structure and Properties of Solid Surface, University of Chicago press, Chicago, 1953.
[6] S. Cuenot, C. Frétigny, S. Demoustier-Champagne, B. Nysten, Physical Review B 69 (2004) 165410.
[7] M. Doyle, T.F. Fuller, J. Newman, Journal of the Electrochemical Society 140 (1993) 1526–1533.
[8] T.F. Fuller, M. Doyle, J. Newman, Journal of the Electrochemical Society 141 (1994) 1–10.
[9] M. Doyle, J. Newman, A.S. Gozdz, C.N. Schmutz, J.-M. Tarascon, Journal of the Electrochemical Society 143 (1996) 1890–1903.
[10] R. Darling, J. Newman, Journal of the Electrochemical Society 144 (1997) 4201–4208.
[11] D.R. Baker, M.W. Verbrugge, Journal of the Electrochemical Society 146 (1999) 2413–2424.
[12] V. Srinivasan, J. Newman, Journal of the Electrochemical Society 151 (2004) A1517–A1529.
[13] S. Devan, V.R. Subramanian, R.E. White, Journal of the Electrochemical Society 151 (2004) A905–A913.
[14] D. Dees, E. Gunen, D. Abraham, A. Jansen, J. Prakash, Journal of the Electrochemical Society 155 (2008) A603–A613.
[15] S. Prussin, Journal of Applied Physics 32 (1961) 1876–1881.
[16] W.L. Wang, S. Lee, J.R. Chen, Journal of Applied Physics 91 (2002) 9584–9590.
[17] S. Lee, W.L. Wang, J.R. Chen, Materials Chemistry and Physics 64 (2000) 123–130.
[18] S.-C. Ko, S. Lee, Y.T. Chou, Materials Science and Engineering A 409 (2005) 145–152.
[19] R.E. Garcia, Y.-M. Chiang, W.C. Carter, P. Limthongkul, C.M. Bishop, Journal of the Electrochemical Society 152 (2005) A255–A263.
[20] J. Christensen, J. Newman, Journal of the Electrochemical Society 153 (2006) A1019–A1030.
[21] J. Christensen, J. Newman, Journal of Solid State Electrochemistry 10 (2006) 293–319.
[22] X. Zhang, A.M. Sastry, W. Shyy, Journal of the Electrochemical Society 155 (2008) A542–A552.
[23] X. Zhang, W. Shyy, A.M. Sastry, Journal of the Electrochemical Society 154 (2007) A910–A916.
[24] Y.-T. Cheng, M.W. Verbrugge, Journal of Applied Physics 104 (2008) 083521–083526;
M.W. Verbrugge, Y.-T. Cheng, Electrochemical Society Transactions 16 (13) (2008) 127–139;
M.W. Verbrugge, Y.-T. Cheng, Journal of Electrochemical Society 156 (2009) A927.
[25] Y.-T. Cheng, M.W. Verbrugge, Journal of Power Sources 190 (2009) 453–460.
[26] P. Sharma, S. Ganti, N. Bhate, Applied Physics Letters 89 (2006) 049901–149901 (Erratum: [Appl. Phys. Lett. [bold 82], 535 (2003)]).
[27] H.S. Carslaw, J.C. Jaeger, Conduction of Heat in Solids, second ed., Clarendon Press, Oxford, 1959.
[28] S. Timoshenko, J.N. Goodier, in: S. Timoshenko, J.N. Goodier (Eds.), Theory of Elasticity, McGraw-Hill, New York, 1951.
[29] J. Crank, The Mathematics of Diffusion, Oxford University Press, USA, 1980.
[30] M.-H. Park, M.G. Kim, J. Joo, K. Kim, J. Kim, S. Ahn, Y. Cui, J. Cho, Nano Letters 9 (2009) 3844–3847.
[31] L.-F. Cui, R. Ruffo, C.K. Chan, H. Peng, Y. Cui, Nano Letters 9 (2008) 491–495.
[32] H. Kim, J. Cho, Nano Letters 8 (2008) 3688–3691.
[33] L.-F. Cui, Y. Yang, C.-M. Hsu, Y. Cui, Nano Letters 9 (2009) 3370–3374.
[34] Y. Li, X. Lv, J. Li, Applied Physics Letters 95 (2009) 113102–113103.
[35] E. Hosono, T. Kudo, I. Honma, H. Matsuda, H. Zhou, Nano Letters 9 (2009) 1045–1051.
[36] E. Hosono, H. Matsuda, I. Honma, S. Fujihara, M. Ichihara, H. Zhou, Journal of Power Sources 182 (2008) 349–352.
[37] R.E. Miller, V.B. Shenoy, Nanotechnology 11 (2000) 139–147.
[38] D. Aurbach, Journal of Power Sources 89 (2000) 206–218.